SPIE Proceedings: Style template and guidelines for authors

Anna A. Author[a] and Barry B. Author[b]

[a]Affiliation1, Address, City, Country
[b]Affiliation2, Address, City, Country

ABSTRACT

TBD

Keywords: Manuscript format, template, SPIE Proceedings, LaTeX

1. INTRODUCTION

The HERMES (High Energy Rapid Modular Ensemble of Satellites) project is based on a revolutionary mission concept based on modular astronomy. More specifically, HERMES is conceived as a constellation of nano/micro/small satellites in low Earth orbits, hosting technologically advanced X/gamma-ray detectors, with relatively small effective area, to localise and investigate the spectral and temporal properties the high-energy emission of bright highly-energetic transient events.

Interestingly, we are now in the middle of a transition phase both scientifically and technologically speaking. On one hand, we recently witness the beginning of the so-called *Multi-messenger Astronomy*, that coincided with the observation of the Gravitational Wave Event GW170817 by the Advanced LIGO/Virgo [1], followed by the detection of the associated short Gamma-Ray Burst (GRB) detected by the Fermi and INTEGRAL satellites [2], as well as the countless follow-up multi-wavelength observations. Immediately after this discovery, it become even clearer for the community the urgency for an high-energy all-sky with good localisation capabilities to work in parallel with gravitational wave observatories such as Ligo/Virgo/Kagra that will reach their final sensitivity within a few years. At the moment, all the available satellites providing the detection and localisation of GRBs have been operational for more than a decade with large chances of decommissioning in the next years, while next-generation large-area detectors will not be available for at least 10-15 years from now.

On the other hand, we are living in the hera where new technologies can finally challenge the current assumptions that high-energy astronomical observations from space can only be achieved by big satellites, usually designed, built, launched and managed by government space agencies. CubeSats, light spacecrafts with small sizes and reduced costs, are now considered a competitive solution for space applications as they allow equilibrium among crucial variables of a space project, such as development time, cost, reliability, mission lifetime, and replacement. Interestingly, they represent the key to realise the revolutionary concept of distributed (modular) space astronomy crucial to investigate the unknown of the Universe. Indeed, the large number of photons required to performe cutting edge (astro)physical space science can be collected adding up the contribution of a large number of astrophysical detectors distributed over a fleet of nano/micro/small-satellites allowing to achieve huge overall collecting areas which otherwise would be unreachable with a single instrument and impossible to carry with the current rocket load capabilities. The decreasing trend of producing costs as well as the increase of launching opportunities witnessed in recent years, allows us to concretely conceive fleets of hundreds/thousands of coordinated satellites acting as a single detector of unprecedented collecting power.

The HERMES Full Constellation (HFC) has been conceived to tackle three main scientific objectives:

- the accurate and prompt localization of bright hard X-ray/soft gamma-ray transients such as GRBs. Fast high-energy transients are among the likely electromagnetic counterparts of the gravitational wave events (GWE) recently discovered by Advanced LIGO/Virgo, and of the Fast Radio Burst;

Further author information: (Send correspondence to A.A.A.)
A.A.A.: E-mail: aaa@tbk2.edu, Telephone: 1 505 123 1234
B.B.A.: E-mail: bba@cmp.com, Telephone: +33 (0)1 98 76 54 32

- Open a new window of timing at X/gamma-ray energies, and thus investigate for the first time the temporal structure of GRBs down to fractions of micro-seconds, to constrain models for the GRB engine;

- Test quantum space-time scenarios by measuring the delay time between GRB photons of different energy.

The determination of the position in the sky of an astrophysical transient source is crucial to investigate its origin. A clear example of that is the case of Gamma Ray Bursts (GRBs, hereinafter). Indeed, for almost thirty years after their discovery, GRBs remained poorly understood due to the lack of precise localization. Only in the late 90s, with the launch of the Italian-Dutch X-ray satellite BeppoSAX (ref), the detection of the GRB X-ray afterglow (van Paradijs, J., et al., 1997 Nature, 386, 686) and the subsequent identification of the optical and radio transient by ground-based telescopes, allowed the identification of the host galaxy and hence its extragalactic origin (see e.g. [3], for a review). This paramount discovery allowed to gauge the energy output of the GRBs, establishing their cosmological nature. GRBs proved to be, eventually, the most powerful electromagnetic explosions in the Universe, one of the best tools to investigate the Universe during its infancy. Similarly, the recent confirmation of short GRBs being the electromagnetic counterparts of a Gravitational Wave Events (see e.g. [1, 2]) made the improvement of localisation capabilities of the astronomical observatories a short term technological priority. Indeed, the key to exploiting the Multi-messenger Astronomy is the fast and accurate identification of the electromagnetic counterparts of GWEs, that is crucial to promptly characterised the properties of these events.

The improved sensibilities of the next generation interferometers, will allow the detection of fainter and further away events, making more challenging the identification of their electromagnetic counterparts given the larger portions of space to be searched. Taking as a reference the famous GW170817 event, the horizon for NS-NS merging events detected with a similar signal to noise will reach up to 200 Mpc for LIGO and 100-130 Mpc for Virgo in a few years from now. This implies an increase of the discovery volume a factor ~100 with respect to the GW170817 case. In this scenario, the operation of an efficient X/gamma-ray all-sky-monitor with good localization capability will have a pivotal role in quickly discovering the high-energy counterparts of GWEs and triggering coordinate multi-wavelength observing campaigns.

Another key aspect of modular astronomy is the possibility to combine together the information collected by single elements of the constellation to increase the signal-to-noise ratio, recreating the capabilities of a single observatory with large collecting area. Indeed, once the transients are detected and localised, the signals received by the different detectors can be combined together, after correcting for the delay time of arrivals, significantly increasing their statistics and thus the sensitivity to finer temporal structures. This aspect is particularly important for events such as GRBs, characterised by huge luminosities and fast variability, often as short as one millisecond. Best most accurate available description of these events is included in the so-called *fireball model*, i.e. a relativistic bulk flow where shocks efficiently accelerate particles. Interestingly, while successful in explaining GRB observations, this model implies a thick photosphere, hampering direct observations of the hidden inner engine that accelerate the bulk flow. One possibility to shed light on their inner engines is through GRB fast variability (see e.g. Kobayashi et al. 1997, ApJ, 490, 92; Morsony et al. 2010, ApJ, 539, 712; Nakar & Piran 2002, ApJ Letters, 572, L139). GRB light-curves have been investigated in detail down to *sim*1 ms or slightly lower (see e.g. Walker et al. 2000, ApJ, 537, 264; MacLachlan et al. 2013, MNRAS, 432, 857), while the μs-ms window is basically unexplored, as little known is also the real duration of the prompt event. We do not know how many shells are ejected from the central engine, which is the frequency of ejection and which is its length. With HFC it will be possible to possible to access the the μs-ms timing window for GRBs, allowing to further investigate their central engines.

The extraordinary capabilities of the HFC will also allow the first dedicated experiment for testing quantum gravity theories. The experiment is based on the predictions of a discrete structure for space on small scales (of the order of the Plack length) proposed by several theories. This space discretization implies the onset of a dispersion relation for photons, as well as an energy dependence of their propagation speed. A promising method for constraining a first order dispersion relation for photons in vacuo is the study of discrepancies in the arrival times of high-energy photons of GRBs emitted at cosmological distances in different energy bands (see e.g. Burderi et al. 2020 and references therein for more details on the topic).

Taking advantage of the modularity of the project, the HERMES concept will be tested following a step-by-step strategy. More specifically, at first it will be realised the HERMES Pathfinder with the aim at proving in space the HERMES concepts, by detecting and localizing GRBs with six units. The successful realization of this experiment will guide the consolidation of the HERMES full constellation design with the final goal to monitor the full sky and provide ¡arcmin localization of most GRBs. The HERMES Pathfinder consist of two different projects: the HERMES Technological
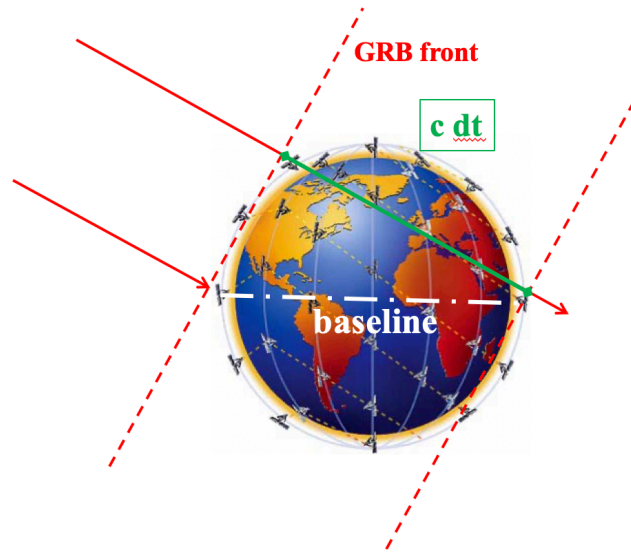
Figure 1. Schematic representation of the *Temporal Triangulation* principle applied to a constellation of CubeSats distributed in low Earth orbits. Red arrows represent the emitted GRB photons, while the red dashed lines describe the travelling GRB front wave at different times. The green segment represents the difference in travelled distances of the GRB photons detected by two CubeSats placed at a generic baseline (white dashed line).

Pathfinder (HTP) and the HERMES Scientific Pathfinder (HSP). The former, funded by the Italian Ministry of University and Research (MIUR) and the Italian Space Agency (ASI), aims at producing three 3U nano-satellites equipped with X/gamma-ray detectors [4,5]. The latter, funded by the European Unions Horizon 2020 Research and Innovation Program, aims at realising three additional units (payload+spacecraft). Moreover, the project includes the design and development the mission and science operation centers (MOC & SOC). The HTP/HSP mini-constellation of six 3U units should provide enough GRB detections and localizations to:

- validate the overall concept as well as study the statistical and systematic uncertainty on both detection and localization to design the full constellation;

- prove that accurate timing in the still little explored window μs-ms is feasible using detectors with relatively small collecting area;

- study uncertainties associated to the addition of the signal from different detectors to improve the statistics on high-resolution time series.

Finally, ASI recently approved and funded the participation to the project SpIRIT (Space Industry Responsive Intelligent Thermal), founded by the Australian Space Agency, and led by University of Melbourne. SpIRIT will host an HERMES-like detector and S-band transmission systems. The HERMES-TP/SP mini-constellation of six satellites plus SpIRIT should be tested in orbit during 2022. More details on the overall HERMES mission description can be find in [6].

2. TRIANGULATION TECHNIQUE

The aim of this work is to investigate the localisation capabilities of the HTP/HSP mini-constellation composed of six 3U units. The main targets that will be discussed in the following are the highly energetic high-energy transients GRBs.

The simple and robust idea that will be applied for accurately localise the transient astrophysical sources is the so-called *Temporal Triangulation*.
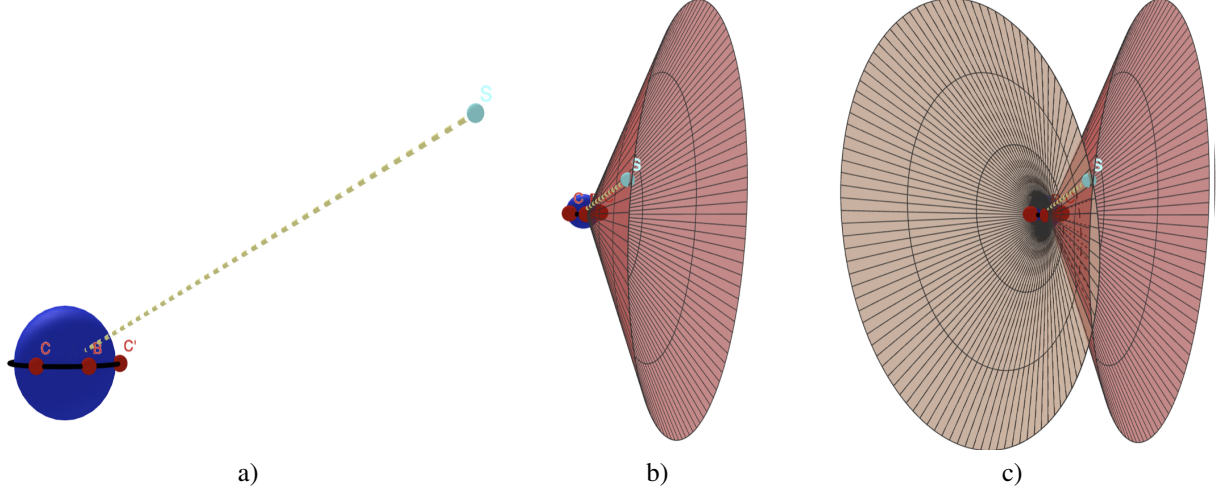
Figure 2. *Panel a)* Schematic representation of a triplet of CubeSats distributed in an equatorial plane that observed simultaneously a transient event located at the position S. *Panel b)* Graphic representation of the infinity source directions identified using the delay measured by combining the observations of the event obtained with the detectors B and C. *Panel C)* Superposition of the source directions obtained combining the delays obtained with the detector paris B-C and B-C'. The intersection of the two cones identifies two possibile locations of the event in the sky.

To describe the principle behind the method, let us represent the transient event as a narrow wavefront (pulse) travelling in a given direction and let us displace a network of detectors in space. The narrow wavefront will hit the detectors of the network at different times that depend on the spatial position of each detector and the direction of the wavefront. As represented in Figure 1, the transient event will be registered by two detectors of the network with a delay *dt* proportional to their projected distance with respect to the source direction (green segment). The combination of the delays measured by different pairs of detectors observing the same event will allow to reconstruct its position in the sky. For the sake of description, let us consider a subset of 3 detectors distributed in the equatorial plane (panel a of Figure 2) observing simultaneously a generic event S in certain position in the sky (with direction with respect to the Earth barycenter represented by the yellow dashed line). As shown in panel b of Figure 2, the delay measured Δt_{BC} by combining the observations of the detectors B and C allows us to identify a set of infinite possible directions of the transient source belonging to a circulare base of a cone. Each of these source directions $\vec{d}_i$ satisfies the relation $\Delta t_{BC} = \vec{\rho}_{BA} \cdot \vec{d}_i$, where $\vec{\rho}_{BA}$ is the vector describing the distance between the two detectors. A similar result can be obtained by combining the measurements of the detectors B and C'. Interestingly, the superposition of these two results reduces the degeneracy in the source direction, allowing us to determine two possible positions of the source defined as the intersections of the two cones (Figure 2 panel c), one of which corresponds (as expected) with the real one. Increasing the number of independent delay measurements, it is then possible to univocally localise the transient event in the sky. It is then clear that in order to achieve localisation capabilities, a generic fleet of the detectors distributed in space should guarantee the simultaneous observation of an event with at least three of its elements.

The description of the method reported so far does not take into account of any possible source of the uncertainty associated with the system. More in detail, the localisation capabilities of the system, hence the accuracy associated with the source position, will depend on several aspects such as the capability of reconstruct the position of the detectors during the observation of the event, the ability to recover the delay between signals observed by different detectors and the capability of the detector to precisely time tag the photons associated with the transient event. A first proxy on the accuracy in determining the source position $_{PA}$ can be determine in the hypothesis of an event (e.g. a GRB) whose emitted photons arrive to a series of N detectors uniformly distributed in an orbit, and it is given by the expression:

$$\sigma_{PA} = \frac{(\sigma_{delay} + \sigma_{tpos} + \sigma_{time})^2}{< Baseline > \sqrt{(N-1-2)}} \tag{1}$$

where σ_{delay} is the error on the delay measurement obtained combining the light-curves recorded by two detectors,

$\sigma_{tpos} = \sigma_{pos}/c$ is the error induced by the uncertainties on the space localisation of the detectors, σ_{time} is the uncertainty on the absolute time reconstruction, $< Baseline >$ is the average distance between the detectors ad $N_{ind} = N - 1$ is the number of statistically independent pairs of satellites used to determine the delay measurements.

For a more accurate approach on determine the position and relative uncertainties of a generic GRB in the sky by means of time delay measurements, let us consider a swarm of n satellites, each one identified by a position vector $\vec{r}_i$ (with $i = 0, \ldots, n - 1$) with respect to a suitable reference frame, e.g. the Earth barycenter in equatorial coordinates. To determine the GRB direction $\hat{d}$, it is possible to measure the time delays of the GRB signal as seen from each pair of satellites. Defining t_0 the time at which the GRB signal arrives at the origin of the chosen reference frame, each i-th satellite will receive the GRB at a time t_i

$$t_i = t_0 - \frac{\vec{r}_i \cdot \hat{d}}{c}. \tag{2}$$

The expected time delays between two satellites will be

$$\Delta t_{ij}(\hat{d}) \equiv t_j - t_i = \frac{(\vec{r}_j - \vec{r}_i) \cdot \hat{d}}{c} = \frac{\vec{\rho}_{ij} \cdot \hat{d}}{c}, \tag{3}$$

where $\vec{\rho}_{ij} \equiv \vec{r}_j - \vec{r}_i$. The real (measured) time delay between the signal recorded by two satellites $\Delta\tau_{ij}$ is inferred e.g. by applying cross-correlation techniques to the light-curves. The direction of the GRB, e.g. its equatorial coordinates, can be estimated comparing the computed and measured delays between satellites using e.g. the non linear least squared method. We define the $\chi^2(\hat{d})$ function as the sum the squares of the difference between the expected and observed time delay divided by its statistical error

$$\chi^2(\hat{d}) = \sum_{i=0}^{n-2} \sum_{j=i+1}^{n-1} \frac{(\Delta\tau_{ij} - \Delta t_{ij}(\hat{d}))^2}{\Theta_{ij}^2}, \tag{4}$$

where Θ_{ij}^2 includes the positional error on the satellites expressed in light-seconds, the accuracy in the absolute timing of the detectors, the uncertainty on constraining the time delay between the signals and any hypothetical systematic uncertainty related to the set-up or method applied.

The unitary vector $\hat{d}$ identifying the GRB direction can be written in terms of Right Ascension α and Declination δ, that is

$$\hat{d} = \{\cos\alpha\cos\delta, \sin\alpha\cos\delta, \sin\delta\}. \tag{5}$$

Minimising Eq. 4 with respect to α and δ gives us an estimate of the direction of the GRB. Moreover, if Eq. 4 satisfies all the hypotheses in [Y. Anvi, 1976, ApJ, 210, 612], we can also calculate the confidence region for the GRB equatorial coordinates on the plane of the sky.

3. EXPLOITING THE HERMES PATHFINDER LOCALISATION CAPABILITIES

In the following, we describe in details the analysis performed, as well as the related assumptions and caveats, to investigate the capabilities of the HERMES-TP/SP mini-constellation (6 3U CubeSats) on localizing GRBs in the sky.

The key to accurately locate an event by means of the temporal triangulation method described above is to decrease as much as possible the uncertainties summarised by the term Θ^2 of Eq.4. Starting from the HTP/SP technical properties, we can investigate the positional uncertainty budget to be able to identify the most crucial limiting factors. The final design of the spacecraft including GPS receivers and accelerometers, guarantees the possibility to reconstruct the position of the CubeSats with an accuracy smaller than 30 meters, that translates into an temporal accuracy lower than 30 ns (see SPIE PoliMi). Moreover, the absolute timing accuracy achievable from the detector is going to be lower than 0.4 μs for both the X and S modes [see SPIE Evangelista]. As we show in more detail later, considering the HERMES-TP/SP set up, we can conclude that, even for the brightest GRBs, the uncertainty on the GRB position will be dominated by the accuracy on the time delay between the GRB light-curves and possibly by unknown systematics still to be investigated. In the following we will show that on average uncertainties on the time delays obtained applying cross-correlation techniques are of the other of tenths of milliseconds, a few orders of magnitude larger than the uncertainties discussed above.

3.1 GRB structure and time delay accuracy

To be able to investigate the achievable accuracy in the measurement of the time delays between the arrival times for photons emitted by a generic GRB and observed by different detectors of the HTP/SP mini-constellation, we built a procedure that includes the creation of GRB templates, the application of cross-correlation techniques as well as Monte Carlo simulations.

As a first step, we searched the available Fermi GBM archive seeking for GRBs characterised by variability on time scales as short as a few milliseconds. The hypothesis being that fast variability should enhance the sensitivity on time delay measurements, especially when the statistics of the available data is relatively limited. We then isolated two candidates, one belonging the so-called short GRBs and the other from the long class. More specifically, the short GRB (id. GRB120323507) has been observed on 2012 March 23, and it is characterised by a t_{90}* duration of ~ 0.4 seconds with a fluence of $\sim 1 \times 10^{-5}$ erg cm^{-2}. On the other hand, the long GRB (id. GRB13052327) has been detected on 2013 May 2, and it is characterised by a t_{90} duration of ~ 24 seconds with a fluence of $\sim 1 \times 10^{-2}$ erg cm^{-2}.

The data collected from the GBM catalogue includes light-curves from the sodium iodide (NaI) scintillators and from the cylindrical bismuth germanate (BGO) scintillators, both having a collecting area of about 125 cm^2. The NaI detectors are sensitive to energies included between few keV up to about 1 MeV, while the BGO detectors cover the energy range 150 keV to 30 MeV. We selected data captured with the so called *Time-tagged event (TTE)* format, where the GRBs are continuously recorded with a time resolution of $2\mu s$, within an time interval that includes 15-30 s of pre-trigger information and about 300 s of data after the trigger time.

To be able to recreate the GRB light-curves as seen by the HTP/SP detectors, we selected the energy range 50-300 keV at which corresponds to the largest effective area of scintillators (around 50 cm^2). For this reason, data collected from the GBM observations has been previously filtered in order to have events only in this energy range.

The need to generate GRB templates (functional forms of the GRB light-curves) comes from two crucial aspects in the procedure follow to investigate the measurement of signal delays: a) flexibility to recreate GRB light-curves independently of the detectors effective area and b) the possibility to simulate GRB light-curves with intrinsically poor statistics.

Indeed, simulations on short time scales (~1 ms) of a unique-like type of transient events such as a GRB, based on observed light-curves, can be challenging when the effective area of the detector is so small that the statistic is fully dominated by Poissonian fluctuations that unavoidably characterised the (quantum) detection process. In particular, if the detected counts within the given time scale is ≤ 1, quantum fluctuations of the order of 100% are expected. If, naively, the number of counts per bin is simply rescaled to account for an increase effective area, these quantum fluctuations can introduce a false imprint of 100% variability with respect to the original signal. No definite cure is available to mitigate this problem, that could be, however, alleviated by rebinning and/or smoothing techniques. Although smoothing techniques allows the creation of light curves for a desired temporal resolution, correlation between subsequent bins is unavoidable. Cross-correlation techniques are strongly biased by this effect, therefore we opted for a more conservative method implying standard rebinning in which the number of photons accumulated in each (variable) bin is fixed. After several trials and Monte-Carlo simulations, we found that 6 photons per bin allows to preserve the signal variability introducing undesired fluctuations not larger than ~30%. Applying this rebinning techniques to the GBM light-curves (at the maximum time resolution of $2\mu s$), we generated a variable bin size light-curves. In order to generate a template usable on any time scale, we linearly interpolated the previous light-curve to create a functional expression (template) for the theoretical light-curves. We note explicitly, that linear interpolation between subsequent bins is the most conservative approach that does not introduce spurious variability on any time scales. For a given temporal bin size, it is then possible to rescale the GRB template previously described in order to match the requested effective area (e.g. that of the HTP/HSP detectors), generating then the expected number of photons within the time bins. In addition, before and after the burst, we rescaled the background on the GRB template to match the nominal background collected the detector as predicted with respect to the CubeSat orbits. Figure 3 shows the templates (red lines) for the long (left panel) and short (right) GRBs generated by following the procedure described above.

Each template represents the model of the GRB we want to simulate, and for this reason it will be used to simulate the light curves observed by each couple of detectors we want to consider. In order to simulate detectors with different overall effective areas, each template has been amplified by a constant factor k that is equal to $k = A_{sim}/A_{GBM}$, where A_{sim} and

---

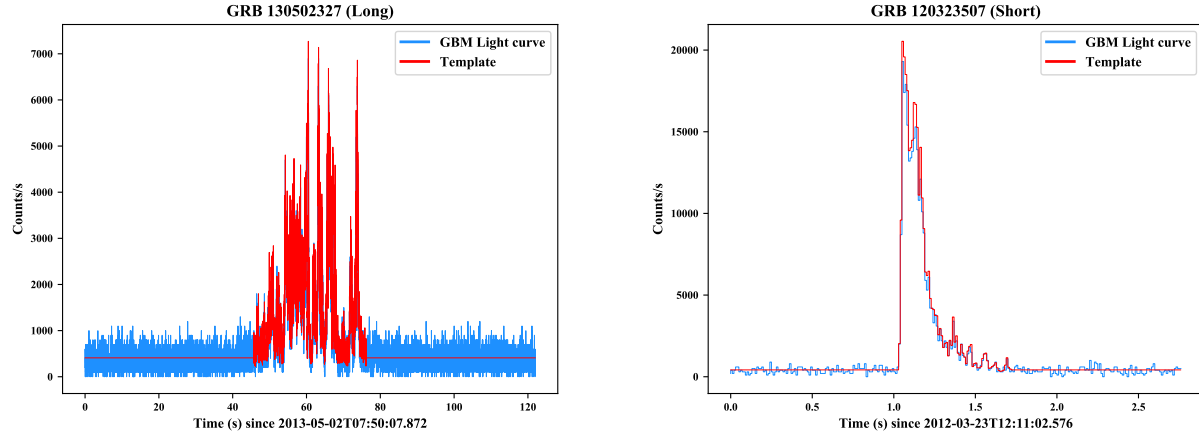*Time interval in which the integrated photon counts increase from 5% to 95% of the total counts.

Figure 3. The Fermi/GBM light curves of the long GRB 130502327 (left panel) and of the short GRB 120323507 (right panel) and the relative *template* (red line) obtained with the procedure described in the text. In both cases, for reasons of clarity, we used a bin time of 10^{-2} s for the light curves and templates of both the GRBs.

A_{GBM} are the areas we want to simulate and that of *GBM*, respectively. The Montecarlo simulations of the light curves of each GRB are successively performed with a Poissonian randomization of the counts contained in each bin of the template. The obtained couple of light curves is then cross-correlated in order to highlight the injected time delay between the curves. In our case, we did not injected a delay between the two signals, then simulating the case in which the couple of detectors is located in the same plane.

The obtained cross correlation profiles are extremely different between each other. The length of the signal is equivalent to the total duration of the analysed light curves but the shape but its variability is strongly related to the complexity of the input light curves and to their intrinsic time variability, as visible in Figure 4. The main peak of this profile returns the value of the time delay for which the pair of input light curves match as much as possible. To obtain the value of this delay, we fitted each profile with an 'ad hoc' function in a limited range of delays around the peak. In the insets of Figure 4, for example, we report a zoom of the peak of the cross-correlation obtained for the long GRB 130502327 and for the short GRB 120323507. In both these cases, this limited part of the cross correlation profile has been fitted with a Gaussian function (red solid line), where the value of the centroid represents the time delay between the light curves collected by the two detectors.

In order to investigate how the accuracy of the measurement for a certain burst is statistically distributed we have to perform Montecarlo simulations of a large number of light curves, as they were collected by detectors with a given collecting area. In addition, it is also considerably interesting to investigate on how this accuracy depends on the area of the detectors, considering both long and short GRBs.

For this reason, we selected a sample of 100 long and short GRBs from the Fermi/GBM archive and chose to perform the analysis taking into account six different areas to simulate for the couple of the detectors: 100 m^2, 50 m^2, 10 m^2, 1 m^2, 0.0125 m^2 (i.e the *GBM* effective area) and 0.0056 m^2 (i.e. the expected area of each HERMES nano-sat).

The sample of GRB we chose is absolutely casual and for this reason is absolutely rapresentative of the wide variety of phenomenologies, fluxes, durations and intrinsic variability that were recorded during the Fermi mission up to the moment in which this paper was written. For the long GRBs we selected bursts having net fluxes ranging between 0.16 and 26 ph cm^{-2} s^{-1}, durations of the bursts between 3 and 138 s, and fluences between 1.67 and 4 ph cm^{-2}. On the other hands, we selected short GRBs with net fluxes between 0.6 and 188 ph cm^{-2} s^{-1}, durations between 0.03 and 1.9 s and fluences between 0.2 and 75 ph cm^{-2}. Just for comparison, in all the *GBM* observations the average value of the background flux is of about 3 ph cm^{-2} s^{-1}.

For each selected burst, and for each considered area we simulated 1000 cross correlation curves (i.e. 1000 couples of light curves of the burst). For each cross correlation profile, as previously shown, we found the injected value of the delay by fitting the peak region with a function that in turn was chosen between a Gaussian function, a composite function consisting in two Gaussian profiles having a common centroid but different σ, a Gaussian function plus an asymmetric double exponential function or alternatively a pure asymmetric double exponential function. Depending on the particular
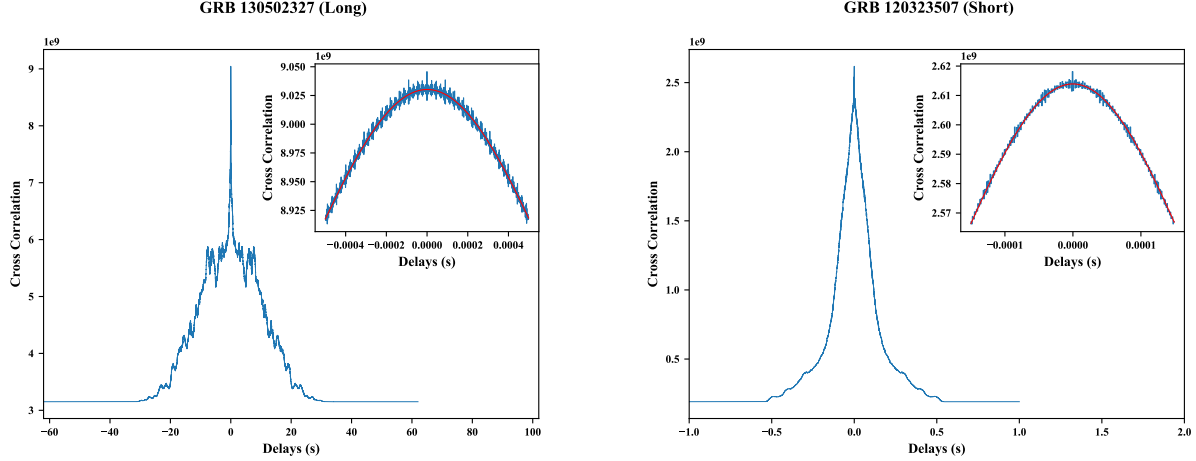
Figure 4. The Cross correlation profiles obtained by simulating the Fermi/GBM light curves of the long GRB 130502327 and of the short GRB 120323507 using the templates shown in Figure 3 for each burst. In each panel we also report an inset showing a zoom of the cross correlation profiles around the peak, and the best fit function resulting by fitting the cross correlation profile in this region with a Gaussian function (red solid line). For the reported cross correlation profiles we used a bin time of $1\mu s$.

shape of the cross correlation profile we chose that function between those listed for which the fit returned the minimum χ^2 value. This analysis has been repeated for both the samples of GRBs (long and short) and for all the considered areas and consisted in 1.2×10^6 couples of simulated light curves from which we obtained the same number of cross correlation profiles, with an overall substantial computational effort that required high storage and computational performances in a multi-core server of 144 logical processors and 504 Gb of RAM.

3.2 Template implementation

Simulations on short time scales (~ 0.1 ms) of a unique type of transient event such as a GRB, based on observed light curves, can be challenging when the effective area of the detector is so small that the statistics are fully dominated by Poissonian fluctuations that unavoidably characterise the (quantum) detection process. In particular, if the detected counts within the given time scale is ≤ 1, quantum fluctuations of the order of 100% are expected. If, naively, the number of counts per bin is simply rescaled to account for an increase of effective area, these quantum fluctuations can introduce a false imprint of 100% variability with respect to the original signal. No definite cure is available to mitigate this problem, that could be, however, alleviated by rebinning and/or smoothing techniques. Although smoothing techniques allow to create light curves for a desired temporal resolution, correlations between subsequent bins is unavoidable. Cross-correlation techniques are strongly biased by this effect, hence we opted for a more conservative method implying standard rebinning in which the number of photons accumulated in each (variable) bin is fixed. After several trials and Monte-Carlo simulations we find that 6 photons per bin allows us to preserve the signal variability introducing undesired fluctuations not larger than ~ 30%. Applying this rebinning technique to the GBM light curves (at the maximum time resolution of $2\mu s$) discussed above, we generated a variable bin size light curve. In order to produce a template for Monte-Carlo simulations, usable on any time scale, we linearly interpolated the previous light curve to create a functional expression (template) for the theoretical light curve. We note explicitly that linear interpolation between subsequent bins is the most conservative approach that does not introduce spurious variability on any time scale.

For a given temporal bin size, we amplified the GRB template previously described in order to take into account the overall effective area of the detector(s) and used this value as the expectation number of photons within the bin. Poissonian randomisation was then applied to produce a simulated light curve. The insets of Fig. **??** show the results of this process for the Long and Short GRB described above simulated for a timescale of 10^{-4} seconds and overall effective area of 100 square meters.

4. DISCUSSION

To obtain a realistic estimation of the accuracy that can be achieved in the measurement of the delays of the arrival times for photons emitted by GRBs in two detectors, we built a method with which we simulated several light curves of different

	Long GRBs			
Area (m^2)	k	a	b	$\chi^2(d.o.f)$
100	-0.2	-56(10)×10^{-7}	20(2)×10^{-6}	5.4×10^{-10}(98)
50	-0.322	-38(6)×10^{-7}	29(2)×10^{-6}	6×10^{-10}(98)
10	-0.216	-134(8)×10^{-7}	49(2)×10^{-6}	4.5×10^{-10}(98)
1	-0.256	-27(2)×10^{-6}	133(5)×10^{-6}	4.3×10^{-9}(98)
0.0125	-0.313	-44(4)×10^{-5}	279(10)×10^{-5}	2×10^{-6}(98)
0.0056	-0.608	-18(7)×10^{-5}	102(4)×10^{-4}	3×10^{-5}(98)

Table 1. Best-fit models obtained by fitting the long GRBs σ vs. fluence profiles with the functional form $y(x) = a + bx^k$. The errors associated to the parameters were evaluated at a confidence level of the 68%.

kinds of GRBs. From a cross correlation of each couple of curves we obtained a measurement of the delay between the two signals that was obtained by fitting the peak of the cross correlation profile with an opportune function.

With a so large sample of GRBs events analysed, a good estimation of the accuracy in determining the delays is given by measuring how for a given typology of burst (long or short) and for each simulated area the centroids distributes around the value of the injected delay. We show the distributions obtained for the long GRB 130502327 and for the short GRB 120323507 in Figure 5. Each delay distribution was fitted with a Normal distribution that allowed to infer a realistic estimation of the delay injected in the simulated light curves and of the dispersion of the delay measurements with respect to the expected value, i.e. a realistic estimation of the cross correlation error E_{cc} defined in Equation 1. This analysis has been repeated for the whole set of areas we simulated and for both the long and short GRBs. In addition, we also compared the mean cross correlation error $< \sigma >$ obtained from the analysis of the delay distributions with the mean value $< \epsilon >$ of the error associated to the centroid obtained from the fit of the cross correlation peak region. We report the results of this analysis in Table 4 and Figure 4 for the long and short data sets of GRBs. From these results it is evident how adopting the ϵ error underestimates the error on the delay measurement via the cross correlation profile, hence resulting in an overestimation of the accuracy in the position of the GRB. In particular, the ratio $< \sigma > / < \epsilon >$ decreases with decreasing the area of the detector as a consequence of the decrement of the statistics of the data collected by smaller areas. For the same reason it is evident how the mean value of σ increases with decreasing the detector area.

More precisely, it is interesting to notice the trend followed by the σ inferred by the fit of the cross correlation profile as a function of the fluence of the GRBs for each simulated area. In Figure 6 and Figure 7 we report these trends for the long and short GRBs considered in our work, respectively. From a quick comparison between the plots in the two figures it can be evinced that the high statistics that can be achieved by the long GRBs, in addition to that characterizing the higher simulated areas for the short GRBs, allows to obtain a more defined profile for the trends, due to the better constraints obtained for the delay measurement in the cross correlation profile. On the contrary, the lower areas, especially for the short GRBs, implied a scattered distribution of the data. However, in both the cases it can be inferred that the error σ on the delay measurement decreases with increasing the fluence of the considered GRB, as a consequence of the increase in the statistics of the data.

We modelled these trends using a functional form as $y(x) = a + bx^k$, where k is a power included between -1 and -0.001. We performed a fit for each k at steps of $\delta k = 1 \times 10^{-4}$ for a total of 9990 fits for each simulated area and GRB typology (long or short); we chose as best-fit function the one having a k for which, together with the a and b parameters, we obtain a minimum of the χ^2. On average, we obtained a minimum of the χ^2 for $k = -0.32$ for all the areas and both for the long and short GRBs, not considering the values of k obtained for the areas 0.0125 m^2 and 0.0056 m^2 simulated for the short GRBs, for which we obtain a considerably flat power of -0.16 and -0.01, respectively, due to the scattered profiles in these two cases. We report the obtained fit parameters in section 4 and Table 4.

ACKNOWLEDGMENTS

Short GRBs				
Area (m^2)	k	a	b	$\chi^2(d.o.f)$
100	-0.304	-57(11)×10^{-7}	159(14)×10^{-7}	8.4×10^{-10}(98)
50	-0.303	-8(2)×10^{-6}	23(2)×10^{-6}	2×10^{-9}(98)
10	-0.325	-17(3)×10^{-6}	49(4)×10^{-6}	8×10^{-9}(98)
1	-0.327	-56(11)×10^{-6}	160(14)×10^{-6}	1×10^{-7}(98)
0.0125	-0.164	-0.011(3)	0.018(3)	0.002(98)
0.0056	-0.010	-0.50(14)	0.52(15)	0.02(98)

Table 2. Best-fit models obtained by fitting the short GRBs σ vs. fluence profiles with the functional form $y(x) = a + bx^k$. The errors associated to the parameters were evaluated at a confidence level of the 68%.

Short GRBs				
Area (m^2)	σ_{min}	σ_{max}	$< \sigma >$	$< \sigma >/< \epsilon >$
100	5.974907063724057e-08	1.8347673286588637e-05	6.534330112671629e-06	7.3457365782627235
50	8.327817977413326e-08	2.8146661479250482e-05	9.21619292355443e-06	6.200167445616318
10	1.867258872028386e-07	6.102888687738298e-05	2.0331103734181935e-05	6.701879256463874
1	5.771539436685253e-07	0.00021081777428695462	6.453042063262608e-05	5.039805652851995
0.0125	9.560084714842066e-06	0.025972208446171898	0.004584209602272932	4.294325462320192
0.0056	1.9398674274012946e-05	0.0787462424572527	0.01360441039839945	4.811604623009573

Table 3. Resume of the results obtained from the simulation of a sample of 100 Short GRBs from the Fermi/GBM archive as a function of the simulated collecting area.

Long GRBs				
Area (m^2)	σ_{min}	σ_{max}	$< \sigma >$	$< \sigma >/< \epsilon >$
100	1.2288202791919088e-07	1.3893084036386532e-05	4.421738574898745e-06	5.163571094402115
50	1.7357168814420108e-07	2.0104233385850118e-05	5.669313287935561e-06	3.2135421748743354
10	3.987123355230972e-07	2.5728427221454894e-05	9.320900692181446e-06	3.2093913438856703
1	1.3132966330242298e-06	7.713557028223853e-05	2.6879835390663862e-05	2.8811619807648956
0.0125	1.798680374494856e-05	0.001739569989617569	0.0004975834853598062	1.3351867706734453
0.0056	3.4300685103588634e-05	0.0063206606110297586	0.001209711899944309	1.252797733846769

Table 4. Resume of the results obtained from the simulation of a sample of 100 Long GRBs from the Fermi/GBM archive as a function of the simulated collecting area.
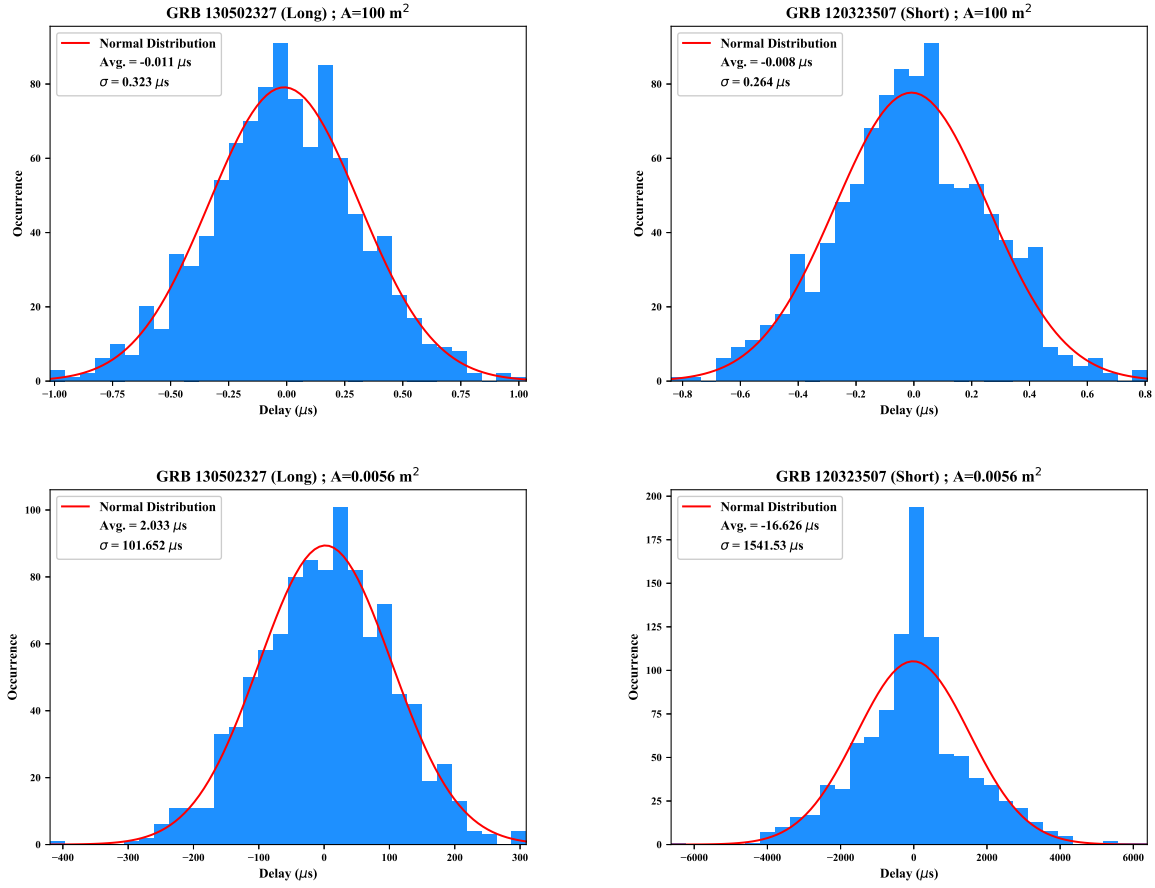
Figure 5. Distributions of the delays obtained for the long GRB 130502327 (left column) and the short GRB 120323507 (right column). For each burst we show a comparison between the results obtained for a simulated area of 100 m² (on the top) and of 0.0056 m² (on the bottom).

REFERENCES

[1] Abbott, B. P., Abbott, R., Abbott, T. D., Acernese, F., Ackley, K., and Adams, C., e. a., "Gravitational Waves and Gamma-Rays from a Binary Neutron Star Merger: GW170817 and GRB 170817A," *Astrophysical Journal, Letters* **848**, L13 (Oct. 2017).

[2] Troja, E., Piro, L., van Eerten, H., Wollaeger, R. T., Im, M., Fox, O. D., Butler, N. R., Cenko, S. B., Sakamoto, T., Fryer, C. L., Ricci, R., Lien, A., Ryan, R. E., Korobkin, O., Lee, S. K., Burgess, J. M., Lee, W. H., Watson, A. M., Choi, C., Covino, S., D'Avanzo, P., Fontes, C. J., González, J. B., Khandrika, H. G., Kim, J., Kim, S. L., Lee, C. U., Lee, H. M., Kutyrev, A., Lim, G., Sánchez-Ramírez, R., Veilleux, S., Wieringa, M. H., and Yoon, Y., "The X-ray counterpart to the gravitational-wave event GW170817," *Nature* **551**, 71–74 (Nov. 2017).

[3] Schilling, G., [*Flash! The Hunt for the Biggest Explosions in the Universe*] (2002).

[4] Fuschino, F. e. a., "An innovative architecture for a wide band transient monitor on board the hermes nano-satellite constellation," *Society of Photo-Optical Instrumentation Engineers (SPIE) Conference Series* (2020).

[5] evangelista, Y. e. a., "The scientific payload on-board the hermes-tp and hermes-sp cubesat missions," *Society of Photo-Optical Instrumentation Engineers (SPIE) Conference Series* (2020).

[6] Fiore, F. e. a., "The hermes-technologic and scientific pathfinder," *Society of Photo-Optical Instrumentation Engineers (SPIE) Conference Series* (2020).
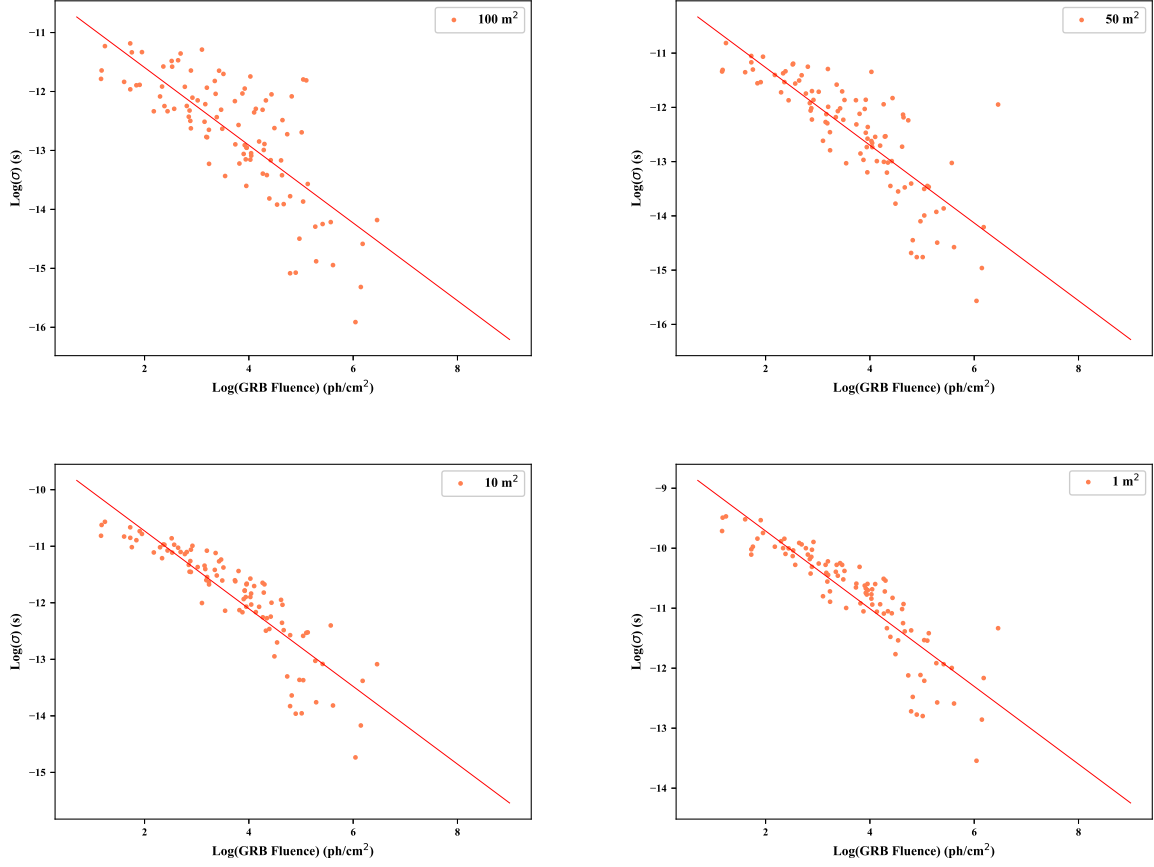
Figure 6. σ of the centroids distribution obtained from the cross correlation curves of the long GRBs, as a function of the GRB fluence for each simulated area. The red solid lines represent the best-fit functions $y(x) = a + bx^k$, where k is the power that minimizes the χ^2, together with the parameters a and b (see section 4 and Table 4 for the parameters obtained for the long and short GRBs, respectively).
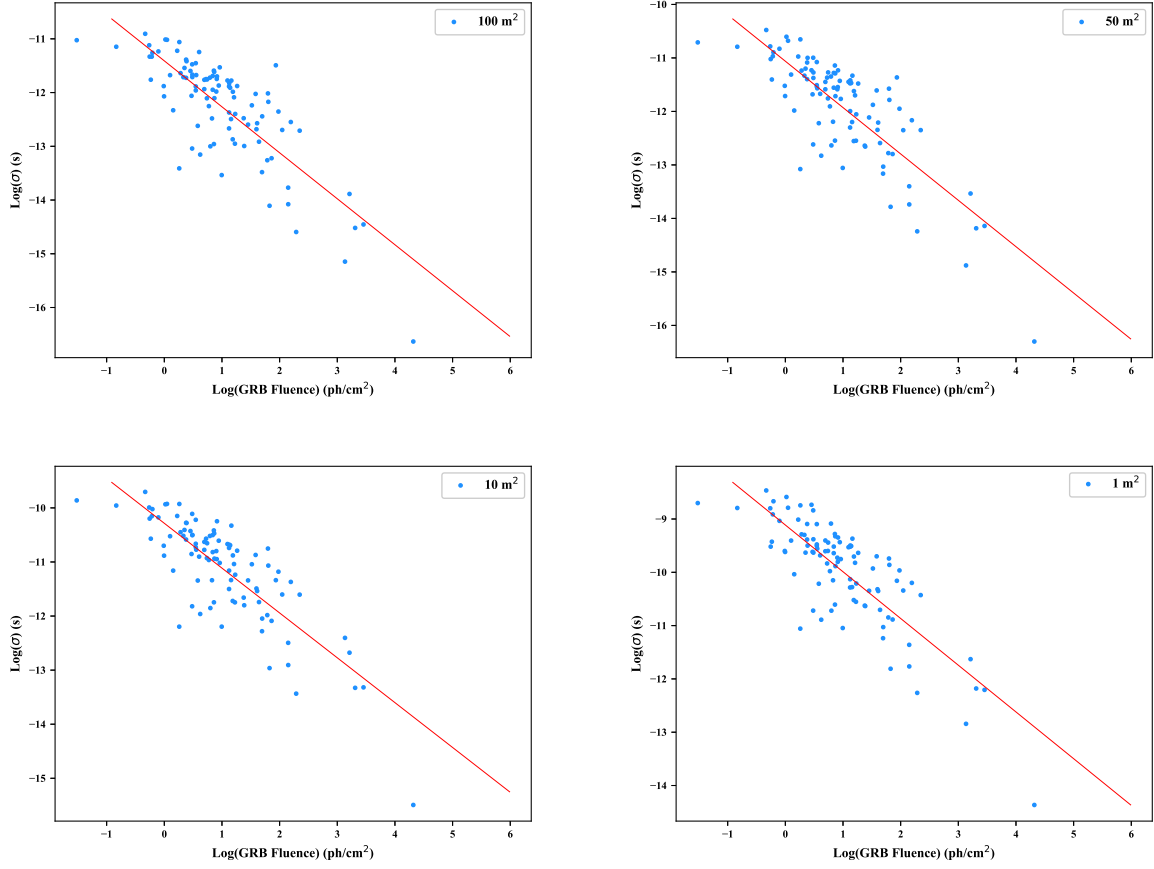
Figure 7. σ of the centroids distribution obtained from the cross correlation curves of the short GRBs, as a function of the GRB fluence for each simulated area. The red solid lines represent the best-fit functions $y(x) = a + bx^k$, where k is the power that minimizes the χ^2, together with the parameters a and b (see section 4 and Table 4 for the parameters obtained for the long and short GRBs, respectively).
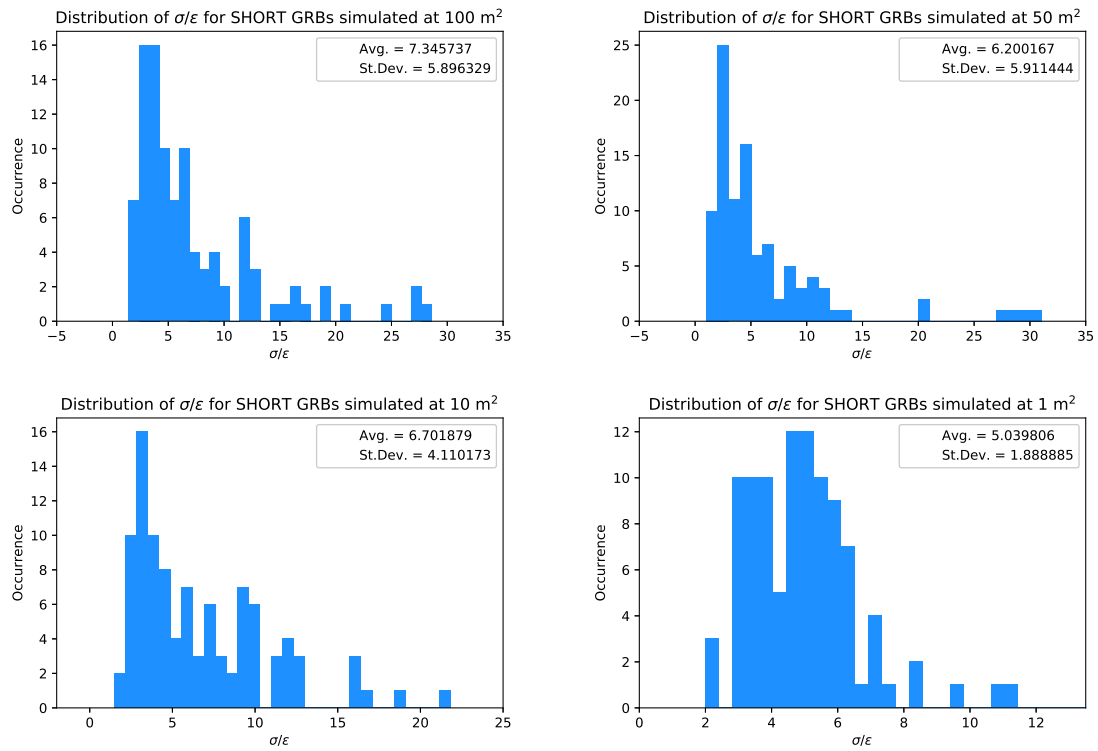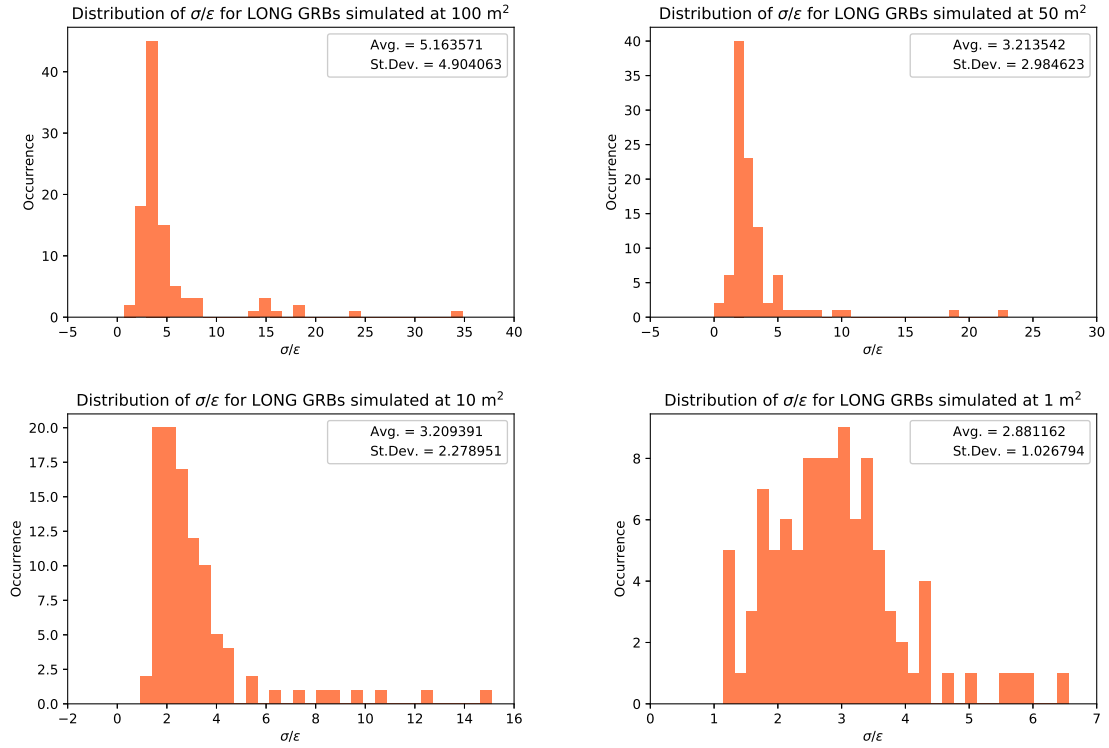
Figure 8. ...

Figure 9. ...

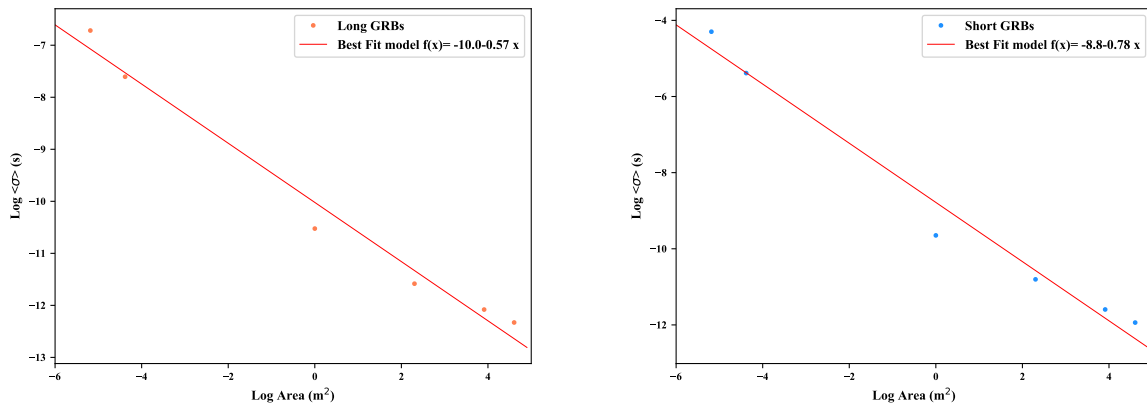Figure 10. Trend of the mean value of the σ obtained for each simulated area as a function of the area of the detector. We also report the best-fit linear function (red solid line) superimposed in each plot.